Bifunctional chimeras of myeloperoxidase and glucose oxidase. Antimicrobial, topological and enzymatic properties

Parfait Kenfack Ymbe, Claire Céré, Brigitte Delord, Gilles Pecastaings, Isabelle Ly, Aurélien Thureau, Laura Rodriguez, Zoran Ivanovic, Véronique Schmitt, Xavier Lafarge, et al.

Journal of Biotechnology 399 (2025) 127–140

Contents lists available at ScienceDirect

Journal of Biotechnology

journal homepage: www.elsevier.com/locate/jbiotec

Bifunctional chimeras of myeloperoxidase and glucose oxidase. Antimicrobial, topological and enzymatic properties

Parfait Kenfack Ymbe [a,1], Claire Céré [a,1,2], Brigitte Delord [a], Gilles Pecastaings [a], Isabelle Ly [a], Aurélien Thureau [b], Laura Rodriguez [c,d], Zoran Ivanovic [c,d], Véronique Schmitt [a], Xavier Lafarge [c,d], Jean-Paul Chapel [a], Claire Stines-Chaumeil [a,*]

[a] CNRS, University of Bordeaux, CRPP, UMR5031, 115 Avenue Schweitzer, Pessac F-33600, France
[b] Synchrotron SOLEIL, HelioBio group, L'Orme des Merisiers, Gif sur-Yvette 91190, France
[c] Établissement français du Sang Nouvelle-Aquitaine, site de Bordeaux Pellegrin, place Amélie-Raba-Léon CS 21010, Bordeaux cedex 33075, France
[d] INSERM U1211 « Maladies Rares: Génétique et Métabolisme », Université de Bordeaux, France

ARTICLE INFO

Keywords:
Infection
Coupled enzymatic system
Multidomain enzyme
Microbicide

ABSTRACT

Enhancing the local substrate concentration is a crucial strategy in nature for facilitating the proximity of two enzymes. The substrate of the first enzyme is transformed into a by-product that travels to the active site of the second enzyme without external diffusion, then transformed into a product and eventually expelled from the complex. In an effort to optimize the antimicrobial properties of myeloperoxidase from *Rhodopirellula baltica* (RbMPO), we created a library of fused chimeras between a glucose oxidase (GOx) and RbMPO so that H_2O_2 could be continuously perfused in the vicinity RbMPO, enabling the production of HOCl or HOSCN, well-known antimicrobial agents. The enzymes were characterized biochemically, enzymatically, and physically using low-resolution techniques such as AFM, SAXS, and cryofracture. SAXS experiments revealed that the chimeras were properly folded and existed in different oligomeric states. The kinetic parameters of the chimeras were determined and used for classification, revealing that all chimeras exhibited varying levels of activity and were microbicidal. The mixture of different oligomeric states of LEGGEAEA displayed both activity and microbicidal properties. AFM was used to visualize the chimeras in different oligomeric states, with their overall shapes ranging from round, oblong, to hooked, depending on the linker used.

1. Introduction

Increasing the local substrate concentration is a key advantage in nature to promote the proximity of two enzymes. The substrate of the first enzyme is transformed into a by-product that travels to the active site of the second enzyme without external diffusion; it is transformed into a product and expelled from the complex. This creates a micro-compartmentalization and a high local concentration of the by-product. Several examples of natural bifunctional enzymes are described in the literature (Zhang, 2011; Khera et al., 2019; Wang et al., 2023; Jiao et al., 2022; Ferraz et al., 2021). This mechanism has been demonstrated for different metabolic pathways such as glycolysis, the Calvin cycle, the pentose phosphate pathway, heme biosynthesis, amino acid synthesis, lipid metabolism, ubiquitination regulation, linalool production etc (Zhang, 2011; Khera et al., 2019; Wang et al., 2023; Jiao et al., 2022; Ferraz et al., 2021). The presence of a channel between the aldolase and aldehyde dehydrogenase of 4-Hydroxy-2-ketovalerate aldolase–aldehyde dehydrogenase (acylating) (DmpFG) has highlighted the importance of sequestering the reaction product to limit volatility and toxicity (Manjasetty et al., 2001, 2003; Smith et al., 2014). Filamentation of alcohol/aldehyde dehydrogenase bifunctional enzyme has been shown essential for substrate channeling and enzymatic regulation (Pony et al., 2020). Theoretical models have also been proposed to study the influence of the proximity of glucose oxidase (GOx)

Abbreviations: AFM, Atomic Force Microscopy; APF, Aminophenylfluorescein; GOx_{Penag}, glucose oxidase from *Penicillium amagasakiense*; IPTG, Isopropyl β-D-1-thiogalactopyranoside; RbMPO, myeloperoxidase from *Rhodopirellula baltica*; TEM, Transmission Electron Microscopy.

* Correspondence to: 115 avenue Albert Schweitzer 33600 PESSAC, France.
E-mail address: claire.stines@crpp.cnrs.fr (C. Stines-Chaumeil).

[1] These two authors contributed equally to this work
[2] PRESENT ADDRESS:INRAE 71 avenue Edouard Bourlaux 33140 Villenave d'Ornon

https://doi.org/10.1016/j.jbiotec.2025.01.018
Received 18 October 2024; Received in revised form 8 January 2025; Accepted 27 January 2025
Available online 28 January 2025

and horseradish peroxidase (HRP) with or without catalase (Kuzmak et al., 2019). The authors showed that cascade reactions were favored if both enzymes (GOx and HRP) were at a distance shorter or equal to 10 nm. Unlike natural bifunctional enzymes, in which the two enzymes of the complex interact, those of chimeras (artificial bifunctional enzymes) are covalently linked, usually by a linker (Reddy Chichili et al., 2013). Genetic engineering is often used to obtain chimeras *via* i) the dockerin/cohesin complex (Lu et al., 2016); ii) enzyme co-immobilization (Arana-Pena et al., 2021); iv) post-translational conjugation (Permana et al., 2021); v) click chemistry with SpyTag/SpyCtacher (Wang and Sun, 2021); v) domain insertion or fusion of protein-coding deoxyribonucleic acid (DNA) (Colpa et al., 2017; Yourno et al., 1970; Bülow et al., 1985). For the fusion of the open reading frame of two enzymes, the introduction of extra sequence between the two open reading frames (ORFs) is possible. Several typical linkers and strategies to optimize their amino acid sequence, their length or their flexibility are described in the literature (Aalbers and Fraaije, 2019; Huang et al., 2021; Gran-Scheuch et al., 2021; Arai, 2021). The size of the linker, i.e. the number of amino acid residues contained in the peptide, is important because it determines the distance between the enzymes of the chimera, and thus the proximity or separation of the active sites. Thus, linker sequences that are short would favor the interaction between the fusion partners, while sequences that are too long would lead to folding problems of the chimeric enzymes. Consequently, a wide range of tests has been performed and, although the efficacy of a specific linker size is not consistently applicable for all fusions, a range of 5–25 amino acid residues is generally appropriate (Cameron et al., 2019; Rabeharindranto et al., 2019). Flexibility depends on the secondary structure the "linker" can adopt after chimera folding. The more flexible the linker, the more likely it is to form random structures; conversely, low flexibility is characterized by a stable secondary structure (usually α-helices). An amino acid such as glycine without a side chain increases the flexibility and solubility of the linker and decreases the potential for interaction with fused enzymes, but increases the probability of interaction between these enzymes. For this reason, less flexible linkers are used by adding hydrophilic amino acids such as lysine, but this increases the likelihood of the Lys side chains interacting with the enzymes (Lu and Feng, 2008; Chen et al., 2013). The third parameter is the linker's physico-chemical properties, conferred by each of its amino acids and its electric charge. Cationic, anionic or neutral linkers are described. Indeed, the presence of Lys or Arg residues gives the peptide a positive charge at physiological pH; conversely, the presence of Glu and Asp residues gives the peptide a negative charge. The neutrality of the peptide can be obtained by using uncharged amino acid residues. Depending on previous investigations on the structures of the enzymes to be fused, this charge may facilitate the reaction mechanism catalyzed by the chimera or reduce possible interactions between the two enzymes.

This description clearly shows that each factor depends on the others and that a synergy must be found between them in order to optimize the use of linkers to fuse enzymes and form efficient bifunctional chimeric enzymes. Kummer *et al.* showed that they obtained a better conversion to the final ethanol product (90 ± 20 %) with a cationic linker chimera compared to the same chimera with a neutral linker (50 ± 20 %) and even compared to the system with each of these enzymes free in solution (20 ± 20 %) (Kummer et al., 2021). Enriched Ser Gly linkers are also showing promising results (Ceballos-Alcantarilla and Merkx, 2021). Chimeric protein for pharmaceutical applications were also studied and reported in the literature (Iyengar et al., 2019). Recently, computational design has also been used to construct chimeras (Ji et al., 2023) and channeling theory has been used to improve dextran production (Zhang et al., 2022).

Once ORF have been fused, another challenge is to produce those multidomain enzymes into multifunctional enzymes.

Myeloperoxidase catalyzes the formation of hypohalogeneous and pseudohypohalogeneous compounds, which exhibit microbicidal and virucidal properties (Cegolon, 2020; Cegolon et al., 2014; El Messaoudi et al., 2002; Chochola et al., 1994). HOCl, in particular, is described as highly reactive compared to H_2O_2 (Schürmann et al., 2017), playing a role in oncogenesis control (Bauer, 2018) and demonstrating non-cytotoxicity (Persoon et al., 2013, 2012). Myeloperoxidase from *Rhodopirellula baltica* is a homolog of human myeloperoxidase (Céré et al., 2023). It offers superior stability and is easier to produce in *E. coli* compared to human myeloperoxidase, as it does not require post-translational modifications. For these reasons, myeloperoxidase was selected for the fusion experiment. The stand-alone GOx was produced into inclusion bodies from heterologous *E. coli* production and then, in a second part of the protocol, folded and reconstituted for several days with FAD in the reconstitution/reactivation solution (Witt et al., 1998). RbMPO was also obtained from inclusion bodies, solubilized in urea and then folded and reconstituted with hemin solution, through several steps of dialysis (Céré et al., 2023). APO enzymes (i.e. without their cofactors FAD or hemin) are inactive and the reconstitution steps with their respective cofactors are essential to activate the activities of the fused enzymes. To verify the efficiency of the reconstitution steps, analysis of the UV–visible spectra and specific profile of APO enzyme compared to the HOLO enzymes could be confirmed. For example, a Soret band appears around 412 nm when RbMPO has been reconstituted with hemin (Céré et al., 2023).

The aim of the present study was to produce an artificial bifunctional enzyme that catalyzes the formation of (pseudo) hypohalogenated compounds from glucose and (pseudo) halides. Scheme 1 explains the catalyzed reactions of the bifunctional enzyme we produced in this study.

We chose to combine the two open reading frame of myeloperoxidase from *Rhodopirellula baltica* and glucose oxidase from *Penicillium amagasakiense* as myeloperoxidase is involved in the innate immune system (Zamocky et al., 2008) and glucose oxidase is used to produce hydrogen peroxide. Genetic engineering experiments resulted in two types of chimera with or without the LEKREAEA peptidyl linker. We demonstrated that the presence of this linker is essential to facilitate the activation of glucose oxidase in the chimera and catalyze the formation of microbicidal compounds sufficient to kill an *Escherichia coli* strain used for antimicrobial resistance testing. Several modifications were performed to the linker to better understand its key properties. For example, (proline) P was introduced, positively or negatively charged amino acids were mutated in G, a longer linker was created and finally, a neutral and flexible linker composed of 8 G was constructed. The sequence and length of the linker proved to be crucial for the topology, oligomerization, kinetics, and microbicidal properties of the chimeras.

2. Results

2.1. Chimera constructions

We employed two approaches to construct the fusion. In the first one, we fused the 3' end of the ORF coding RbMPO with the 5' extremity of the ORF coding GOx using PCR. In the second, we performed a subcloning using *Xho*I as a restriction enzyme, which introduced 24 additional nucleotides between the two ORFs. These nucleotides encoded the LEKREAEA peptidyl linker, which was discovered serendipitously. A comparison of the results from these two constructs (with or without LEKREAEA linker) showed that the linker was crucial for demonstrating microbicidal properties (Figure S11A). To further study the physicochemical properties of this "original" linker, we mutated its sequence and analyzed variants with positively charged, negatively charged, neutral, bent, or longer (16 amino acids) linkers. This allowed us to study in detail the importance of linker's sequence and the role of each amino acid. Seven constructs were obtained with or without linkers between the two open reading frames coding RbMPO and GOx_{Penag}, respectively in Nterminal part and in Cterminal part of the chimera, coding respectively: LEKREAEA, LEKRPEAEA, LEKREAEALEKREAEA,

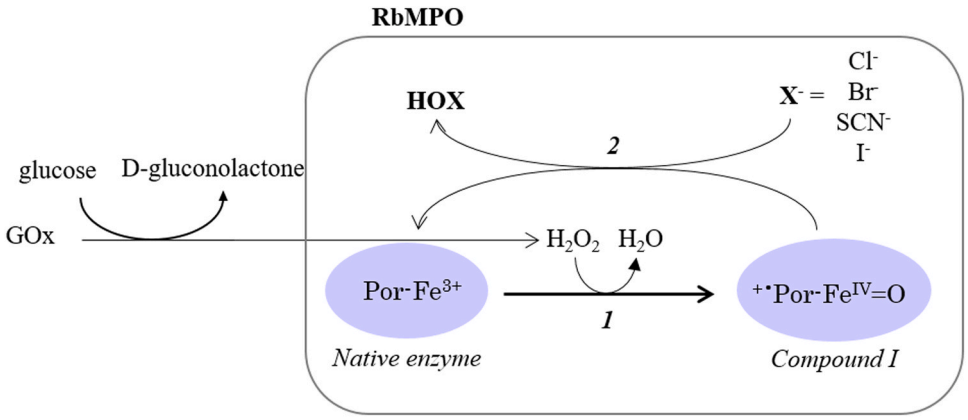

Scheme 1. Schematic representation of the reactions catalyzed by a bifunctional enzyme containing myeloperoxidase from *Rhodopirellula baltica* (RbMPO) and glucose oxidase from *Penicillium amagasakiense* (GOx) activities.

LEGGEAEA, LGKRGAGA or GGGGGGGG. Proteins obtained from these different constructs will be named from the linker sequence [linker peptidic sequence] in the following text or WO for "without linker". For instance, WO or LEKREAEA refers to NterRbMPO-GOxCter or NterRbMPO-LEKREAEA-GOxCter, respectively. Table 1 provides a list of all the constructs studied in this work including, their oligomeric states, which were isolated and tested for their GOx, RbMPO and combined activities.

2.2. Production and purification

The enzyme was produced in the inclusion bodies. Pellets obtained after centrifugation of crude extract were washed with 2 M urea. After incubation with 8 M urea and centrifugation, a band on SDS PAGE around 142 kDa was observed for each chimera in the supernatant (Figure S1A). Additionally, as shown in Figure S1B, the analysis of the various centrifugations and washing steps reveals that the chimera was absent from the supernatant after cell disruption. After treatment with 8 M urea, 40 mg of inclusion bodies were recovered, representing 1 % of the total proteins content the acellular extract of *E. coli* in our production conditions, as estimated by spectral analysis, protein assays and Image J gel quantification software. This shows that the enzyme was pure before the chromatography step. Due to the purity of the chimera before injection on S200 as shown in Figure S1, calibration with standard proteins (Figure S2H) enabled the oligomeric states of the chimera to be determined as a function of their elution volume (Figure S3). Figure S2 A to F (SI) shows the chromatograms obtained during the purification of the chimera. All chimeras were purified after 8 days of reconstitution during which enzymes were incubated with their FAD cofactor and heme prosthetic group under diluted conditions, at 4°C and with gentle agitation. Around 40 mg of enzyme were obtained per 200 mL of culture. Depending of the chimera linker sequence, one or more peaks were detected during the process of purification. In size exclusion chromatography, the first peak corresponds to molecules with a higher molecular weight than those contained in subsequent peaks. Free flavine adenine dinucleotide (FAD) molecules and other components of the reconstitution solution were eluted in the total volume of the S200 column. Seven chimeras, with or without various linkers, were purified and, depending on their elution volume, 19 different proteins at different oligomeric states were analysed and studied. The oligomeric

Table 1
Overview of the constructs used in this study, including their oligomeric state and the activities assessed.

Chimera constructs	Isolated Oligomeric state (n[a]≥1)	GOx[b]	RbMPO[c]	Chimera[d]	Chimera[e]
WO	multimer	x	x	n.d.	x
	monomer	x	x	x	x
LEKREAEA	trimer	x	x	x	x
LEKRPEAEA	multimer	x	x	x	x
	trimer	x	x	x	x
	dimer/monomer	x	x	x	x
LEKREAEALEKREAEA	multimer	x	x	x	x
	trimer	x	x	x	x
	dimer/monomer	x	x	x	x
LEGGEAEA	multimer	x	n.d.	x	x
	dimer/monomer	x	n.d.	x	x
	monomer	x	x	x	x
LGKRGAGA	multimer	x	n.d.	x	x
	trimer	x	n.d.	x	x
	dimer/monomer	x	n.d.	x	x
GGGGGGGG	multimer	x	x	x	x
	trimer	x	x	x	x
	dimer/monomer	x	x	x	x
	monomer	x	x	x	x

x indicates that the measurement was performed
[a] corresponds to the number of monomers in the chimera
[b] refers to the measurement of GOx activity in the chimera, determined using a Megazym kit to monitor the gluconolactone production
[c] denotes the measurement of RbMPO activity in the chimera, assessed using APF fluorescent probe with the addition of H_2O_2 but without glucose
[d] corresponds to the measurement of chimera activity using APF fluorescent probe with varying concentrations of glucose and a fixed concentration of NaCl
[e] corresponds to the measurement of chimera activity using APF fluorescent probe with varying concentration of NaCl and a fixed concentration of glucose; n.d. indicates "not determined"

states as a function of the chimera are summarized in Table S1 and UV–visible spectra are shown in Figure S4. The spectrum of free heme (RbMPO prosthetic group) exhibits two characteristic peaks, one at 385 nm and the other at 615 nm. For the chimera, the heme fixation in the active site is demonstrated by the shift of two peaks to the right of the spectrum at 412 nm and 637 nm respectively. For the peak at 280 nm, a shoulder on the left of the spectrum at 260 nm is observed. These spectra provide several pieces of information: Reinheitszahl (R_z ($\frac{A_{412nm}}{A_{280nm}}$)) is the ratio of absorbance (A) due to the hemin in the Soret band ($A_{412\ nm}$) to absorbance due to the protein ($A_{280\ nm}$), the ratio ($\frac{A_{280nm}}{A_{260nm}}$) and the mass percentage of each enzymes have been calculated for each oligomeric state. These parameters are summarized in Table S1. Rz corresponds to the ratio ($\frac{A_{412nm}}{A_{280nm}}$) is used as a purity parameter for human myeloperoxidase samples. The higher the value, the purer the sample (Andrews and Krinsky, 1981), but it depends on the molecular structure of the enzyme and may vary depending on whether it is a native or recombinant enzyme (Cao and Cheng, 2022). In the case of myeloperoxidase from *R. baltica*, Rz was representative of the correct folding and positioning of the heme of the active site. The ratio ($\frac{A_{280nm}}{A_{260nm}}$) assesses the purity of enzymes towards DNA, or could reflect the presence of FAD in the active site of GOx. We hypothesise that the Soret band observed at 412 nm masks the FAD absorption at 460 nm. Qualitatively, the proteins have a color between yellow and brown, corresponding to an intermediate color between the stand-alone RbMPO (rust brown) or GOx (yellow).

To verify the globular and folded appearance of the chimera and validate the SEC analyses, a model was first obtained on alphafold 3 (Abramson et al., 2024) (Fig. 1A), followed by SAXS experiments (Receveur-Brechot and Durand, 2012) (Fig. 1B and C and Figure S5). SAXS calibration was first performed on lysozyme (whose mass is precisely determined (14500 g/mol)), showing that lysozyme is an enzymatic globular protein with an Rg of 1.6 nm (Figure S5A, A'), in line with previous studies (Phan-Xuan et al., 2020). In a second step, we used this calibration to determine the molecular weight (Mw) of stand-alone enzymes that composed the chimera (Figure S5B, B' and C, C') (Mylonas and Svergun, 2007). SAXS experiments were then carried out on GOx, a folded protein known to be a dimer with an Rg of 3.5 nm in perfect agreement with our measurements (Witt et al., 1998) and an Mw of 132 kg/mol, confirming its dimeric form. Finally, monomers and dimers in line with SEC on LEGGEAEA gave the results in Fig. 1 or Figure S5D and D′ showing compact multidomain proteins composed of GOx and RbMPO with Mws of 168 kg/mol and 360 kg/mol for the monomer and dimer respectively. Alphafold 3 was used to predict multimeric organization (Fig. 1D and E) (Abramson et al., 2024). The predicted template modeling (pTM) score and the interface predicted template modeling (ipTM) score are both derived from the template modeling (TM) score, which measures the overall accuracy of the predicted structure. A pTM score above 0.5 indicates that predicted fold of the complex may resemble the true structure. The ipTM score assesses the accuracy of the predicted relative positions of the monomers within the oligomer. However, predicting the 3D structure of large proteins, especially for oligomers, can reduce the reliability of the model. According to the models observed on Pymol, dimer, or trimer formations show that 70–90 % of the polar interactions between the GOx domains, while 30–10 % of the interactions are between the RbMPO domains of each monomer. This suggests that the GOx domain is the primary site for dimerization, which the RbMPO-RbMPO interaction helping to stabilize the model. These results, along with the RbMPO-RbMPO prediction

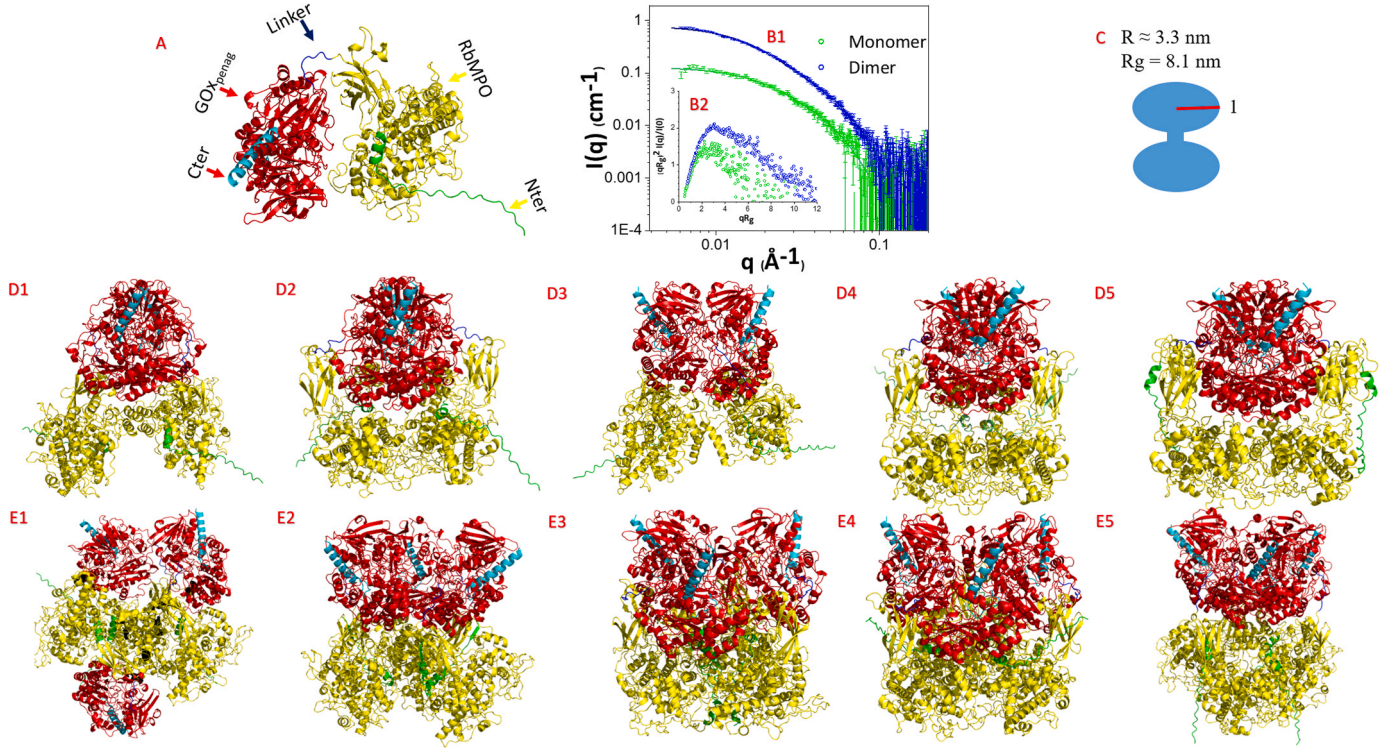

Fig. 1. A) *In silico* prediction 3D structure of LEGGEAEA using AlphaFold3 (Abramson et al., 2024). This model represents a monomer of chimera composed of one RbMPO domain and one GOx domain with the Nter, Cter, and linker sequence labelled (pTM = 0.6); **B1)** SAXS signature on a monomer or a dimer of LEGGEAEA (as hypothesised by SEC experiment) and **B2)** normalised Kratky plot (by the Rg determined using the Guinier approximation at small q where $I(q) \approx I(0)e^{-q^2R_g^2/3}$) showing a folded multidomain structure of the monomer and the dimer **C)** simple form factor (pearl necklace) used to adjust the data. *In* silico 3D structure prediction of LEGGEAEA using AlphaFold 3 for dimeric state, ordered by the interface predicted (ip) and predicted (p) template modeling (TM) scores: **D1**) ipTM = 0.5, pTM= 0.53; **D2)** ipTM = 0.49, pTM= 0.51; **D3)** ipTM = 0.5, pTM= 0.52; **D4)** ipTM = 0.49, pTM= 0.52; **D5)** ipTM = 0.49, pTM= 0.51. *In* silico 3D structure prediction of LEGGEAEA using AlphaFold 3 for the trimeric state ordered by the template modeling (TM) score **E1**) ipTM = 0.39, pTM= 0.45; **E2)** ipTM = 0.39, pTM= 0.45; **E3)** ipTM = 0.38, pTM= 0.45; **E4)** ipTM = 0.38, pTM= 0.45; **E5)** ipTM = 0.38, pTM= 0.44.

data, suggest that GOx-GOx oligomerization is more favorable for chimeric multimers due to reduced steric hindrance. It is also noteworthy that for both the predicted dimeric and trimeric structures, the catalytic sites of the GOx remain intact in the chimera.

2.3. Enzyme characterization of individual active site

Two enzymatic tests were carried out to determine the activity of the two active sites independently of each other.

2.3.1. GOx_{penag}

The Megazyme kit was used to measure the production of D-gluconolactone by GOx_{penag} in end-point mode, specifically to determine the specific activity of the 1st active site of the chimeras. The enzymes were mixed with glucose under optimal time, pH, temperature, and buffer conditions, and the reaction was stopped by the addition of NaOH to increase the pH. D-gluconolactone is then converted into D-gluconate, which can be quantified using a coupled enzymatic system. This process is easily monitored by absorbance measurement at 340 nm, which corresponds to nicotinamide adenine dinucleotide phosphate (NADPH) production as illustrated in Figure S6. The test was performed at pH6, known to be optimal for GOx_{penag} (Courjean and Mano, 2011) and enzyme were incubated during 17 H. By calculating $\Delta A_{340\ nm}$ (experiment minus blank), the concentration of D-gluconate produced by the chimeras could be determined, allowing for the deduction of the specific activity of the different enzymes. This based on the fact that one mole of NADPH produced corresponds to one mole of D-gluconate in the solution which in turns corresponds to one mole of D-gluconolactone produced by GOx (for details see in Material and methods section). The results are presented in Fig. 2A as a histogram and semilog scale to visualize the different activity levels between the chimera and the native GOx. The reference native GOx dimer is highly active, as described previously (Courjean et al., 2010) with a specific activity around 800 U/mg.

The most active enzyme was found to be LEKREAEA with a specific activity of 2.46 ± 0.24 IU/mg followed by the monomer LEGGEAEA (0.73 ± 0.03 IU/mg), then GGGGGGGG the trimer (0.64 ± 0.15 IU/mg) then LGKRGAGA trimer (0.44 ± 0.01 IU/mg), then the trimer

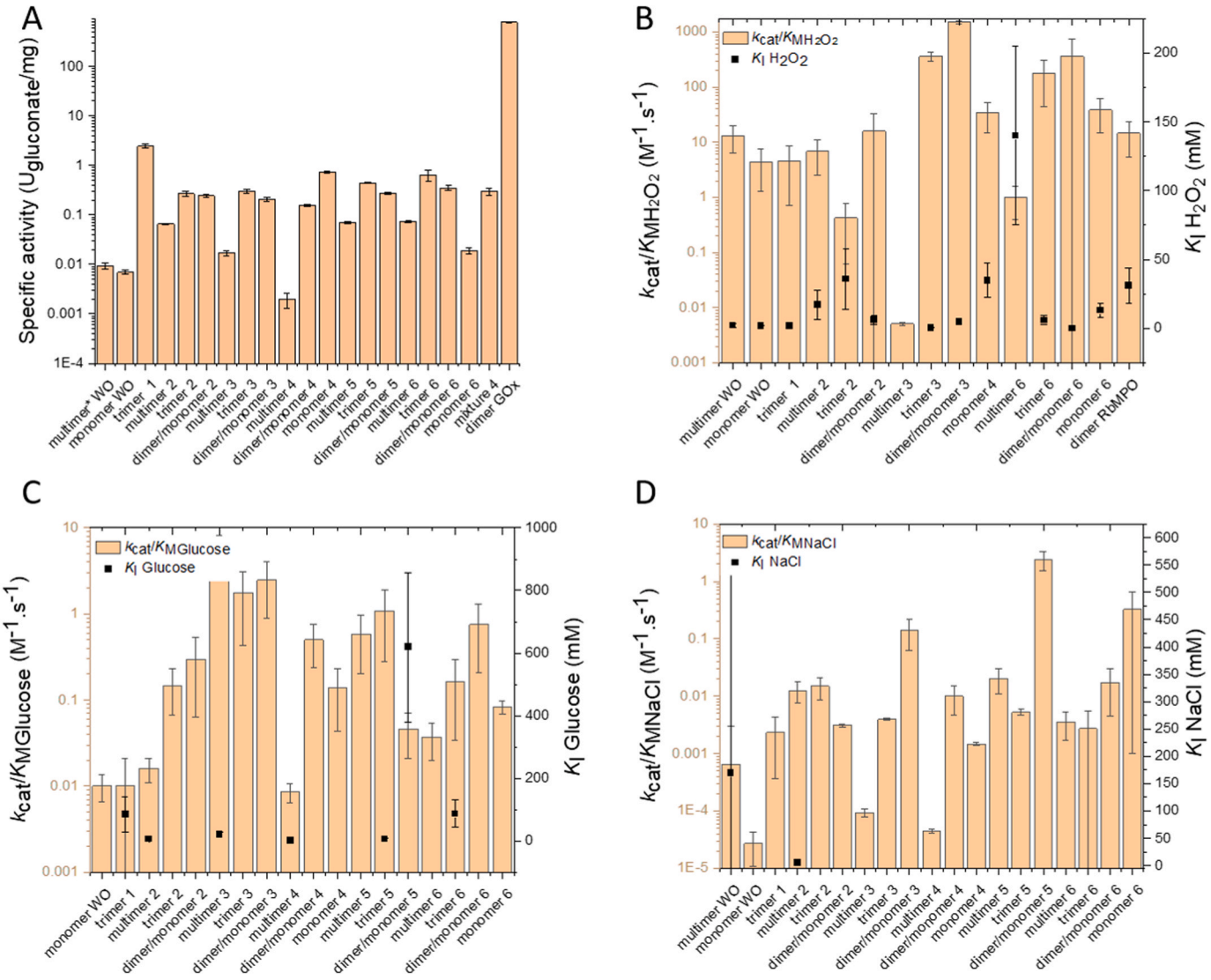

Fig. 2. GOx, RbMPO and chimera activities. A) Glucose oxidase activity. * Test has been carried out at pH 7.5 and for 30 min at 37°C. B) Chlorination efficiency by addition of H_2O_2 at several concentrations: evaluation of k_{cat}/K_{MH2O2} and K_I of H_2O_2. C) Chlorination efficiency by addition of several concentrations of glucose and at fixed concentration of 500 mM NaCl and K_I of glucose. D) Chlorination efficiency at several concentrations of NaCl and at fixed concentration of 20 mM glucose and K_I of NaCl. All tests were performed in at least triplicate. "±" means Mean Standard Error. In the graph, chimera were named WO, 1 for LEKREAEA, 2 for LEKRPEAEA, 3 for LEKREAEALEKREAEA, 4 for LEGGEAEA, 5 for LGKRGAGA and 6 for GGGGGGGG.

LEKRPEAEA (0.27 ± 0.03 IU/mg) and finally the monomer LEKREAEALEKREAEA (0.02 ± 0.01 IU/mg), the latter having the lowest apparent specific GOx activity of all chimeras irrespective of their oligomeric state. These results suggest that the Linker difference in each chimera has an influence on their activities. In addition, we found that, depending on the oligomeric state, the same chimera exhibits different activity.

2.3.2. RbMPO

To determine the RbMPO activity of the chimeras, an H_2O_2 range was run at a fixed concentration of NaCl. HOCl reacted with the aminophenylfluorescein (APF) probe and the appearance of fluorescein was monitored.

Table S2 summarize the steady-state kinetic parameters concerning the chlorination activity of RbMPO inside the chimera and Fig. 2B shown histogram with the $\frac{k_{cat}}{K_M}$ ratios and K_I when enzymes are inhibited by excess H_2O_2. All curves are presented in Figure S7 and all the chimeras tested displayed a chlorination activity, albeit with different efficiency. Due to strong inhibition by H_2O_2, the error bars of the catalytic efficiency for the two chimeras GGGGGGGG and LEKREAEALEKREAEA were very high, so no conclusion could be drawn for this two enzymes. Furthermore, looking at the most active oligomeric state for each chimera, we note that LEKRPEAEA and LEGGEAEA monomer had a high catalytic efficiency (respectively 36 ± 22 and $34 \pm 19\ M^{-1}.s^{-1}$) compared to other chimeras and low inhibition by H_2O_2 ($Ki = 35 \pm 13$ mM), then LEKRPEAEA multimer ($\frac{k_{cat}}{K_M} = 7 \pm 4\ M^{-1}.s^{-1}$) with a slightly higher inhibition ($Ki = 17 \pm 11$ mM), followed by the GGGGGGGG multimer with a low catalytic efficiency ($1.0 \pm 0.6\ M^{-1}.s^{-1}$) but very low substrate inhibition ($Ki = 140 \pm 66$ mM). RbMPO inside the WO monomer was active with an average catalytic efficiency of $4 \pm 3\ M^{-1}.s^{-1}$. Finally, the WO multimer showed a high k_{cat}/K_M ratio due to a low K_M, but the enzyme was strongly inhibited by excess H_2O_2 with the lowest K_I. From these results, we can conclude that each of the chimeras, depending on the presence or absence of a linker, has a catalytic efficiency different from the others. Moreover, as observed for GOx activity in the previous section, LEGGEAEA monomer was one of the most active of all chimeras for chlorination activity and showed low inhibition by excess H_2O_2.

2.4. Enzymatic characterization of the chimera with coupled active site

Measuring the activity of the chimera is complex, as the enzyme has several substrates (Scheme 1).

To switch on the system, glucose and O_2 are the first substrates, which enables GOx_{penag} to produce of H_2O_2, then (pseudo)- halides are the substrates of RbMPO to produce microbicidal compounds such as $^-$OSCN, $^-$OBr, $^-$OCl and $^-$OI. The aim was to measure HOCl production from glucose and NaCl as substrates with the APF probe. Two types of kinetics were performed: i) kinetics at various glucose concentrations and a fixed NaCl concentration and ii) kinetics at different NaCl concentration and a fixed glucose concentration. Steady-state kinetic parameters have been synthetized in Fig. 2C and D, which summarize the $\frac{k_{cat}}{K_M}$ ratios and K_i when the enzymes are inhibited by excess glucose or NaCl substrate. All curves were presented in Figure S8 and S9 and kinetic parameters were summarized in Table S3 and S4. The results obtained differ from one chimera to another.

Firstly, without linker, the chimera is the least effective against both glucose and NaCl.

Excess glucose did not affect all chimeras in the same way, depending on their oligomeric state. The LEKREAEALEKREAEA dimer/monomer was found to exhibit the highest catalytic efficiency ($2.47 \pm 1.58\ M^{-1}.s^{-1}$) and trimer ($1.77 \pm 1.34\ M^{-1}.s^{-1}$), followed by the LGKRGAGA trimer ($1.1 \pm 0.8\ M^{-1}.s^{-1}$) with strong inhibition ($Ki = 6.1 \pm 1.2$ mM), then GGGGGGGG dimer/monomer ($0.75 \pm 0.58\ M^{-1}.s^{-1}$), then the LEKRPEAEA trimer ($0.14 \pm 0.08\ M^{-1}.s^{-1}$) and finally the LEKREAEA trimer ($0.010 \pm 0.011\ M^{-1}.s^{-1}$). Thus, the bifunctional activity of HOCl production from glucose and NaCl differed according to the studied chimera and its oligomeric state. Moreover, the multimer had the lowest activity within each chimera. Concerning the effect of excess NaCl on chimeric activity, only the WO multimer and LEKRPEAEA multimer were inhibited by excess NaCl. Comparing the oligomeric states with the best catalytic efficiency for each chimera, the LGKRGAGA dimer/monomer ($2.4 \pm 0.9\ M^{-1}.s^{-1}$) has the highest efficiency, followed by the LEKREAEALEKREAEA dimer/monomer ($0.14 \pm 0.07\ M^{-1}.s^{-1}$), then the LEKRPEAEA trimer ($0.015 \pm 0.006\ M^{-1}.s^{-1}$), then LEKREAEA trimer ($0.0023 \pm 0.0019\ M^{-1}.s^{-1}$) and finally the LEGGEAEA monomer 1 with $k_2 = 0.0015 \pm 0.0001\ M^{-1}.s^{-1}$ (k_2 was a second-order constant corresponding to the k_{ss}/[NaCl] ratio). Due to large error bars, the catalytic efficiencies of GGGGGGGG cannot be exploited. So, as with the previous activity tests, we observed that in addition to the influence of the linker, there was an influence of the oligomeric state on the activity of each chimera. On the other hand, in this test, the multimers did not always have the lowest efficiency, and we note that the most active chimeras when glucose concentration is varied are not always the same as when NaCl concentration is varied. Taken together, these activity tests show that the linker has an influence on the enzymatic activity of the chimeras, as well as their oligomeric state. Nevertheless, all chimeras have activities.

2.4.1. Microbicidal assays

RbMPO has previously been described to catalyse the transformation of several pseudo- halogenated substrates such as SCN^-, Cl^-, Br^- or I^- (Céré et al., 2023). The activity of LEGGEAEA's monomeric form towards SCN^- was verified (Figure S10) and the chimera was found to be effective with a k_{cat}/K_M ratio of $1427 \pm 310\ M^{-1}.s^{-1}$. To prove the microbicidal activities of the chimeras, microbicidal assays against *E. coli* American Type Culture Collection (ATCC25922) were performed under two experimental conditions: i) in Tryptic Soy Broth (TSB) medium containing 15 mM glucose and 80 mM NaCl and ii) in TSB medium containing 15 mM glucose and supplemented with 25 mM SCN^-. A preliminary study showed that without linker, no antimicrobial effect was observed (Figure S11A) and the effect of HOCl was verify for each experiments (Figure S11B). Also, Figure S11C showed the non microbicidal effect of stand-alone enzyme. Figure S11C shows a 3D graph with varying concentrations of RbMPO (0–1 μM) and GOx (0–25 nM) alongside the kinetic growth of the *E. coli* ATCC25922 strain measured at 620 nm. To achieve a 1:1 molar ratio of non-linked RbMPO and GOx, the concentration of RbMPO had to be reduced between 0 and 25 nM. At higher concentrations of GOx, H_2O_2 inhibited the growth of the *E. coli* strain (Figure S11D), due to H_2O_2 production (Figure S11E), making it difficult to demonstrate the benefit of RbMPO. Therefore, Figure S11 indicates that a molar excess of RbMPO was necessary to showcase its advantage in creating a microbicide-coupled enzymatic system but the efficacy was low compared to chimera. A 1:1 molar ratio was not microbicidal at 25 nM. The GOx of chimera was less active than the stand-alone GOx to be microbicide but produced sufficient H_2O_2 to provide substrate to RbMPO. Microbicidal experiments were then performed with the chimeras that appeared to display the most effective catalytic efficiencies towards glucose and chloride, namely: LEGGEAEA, LGKRGAGA, and LEKREAEALEKREAEA. LEGGEAEA and LGKRGAGA were also of interest due to their low inhibition by H_2O_2. To complete the study, different oligomeric states of these chimeras were assessed. As shown in Fig. 3A to L, all these chimeras inhibited bacterial growth in the presence of either NaSCN or NaCl. Interestingly, this microbicidal effect was observed after storage of the chimeras at 4°C for 4–21 days, demonstrating the stability of these chimeras.

2.4.2. Study of the chimera topology

With the objectives to link the structure and function of the different chimeras, several chimeras were observed either by Cryofracture

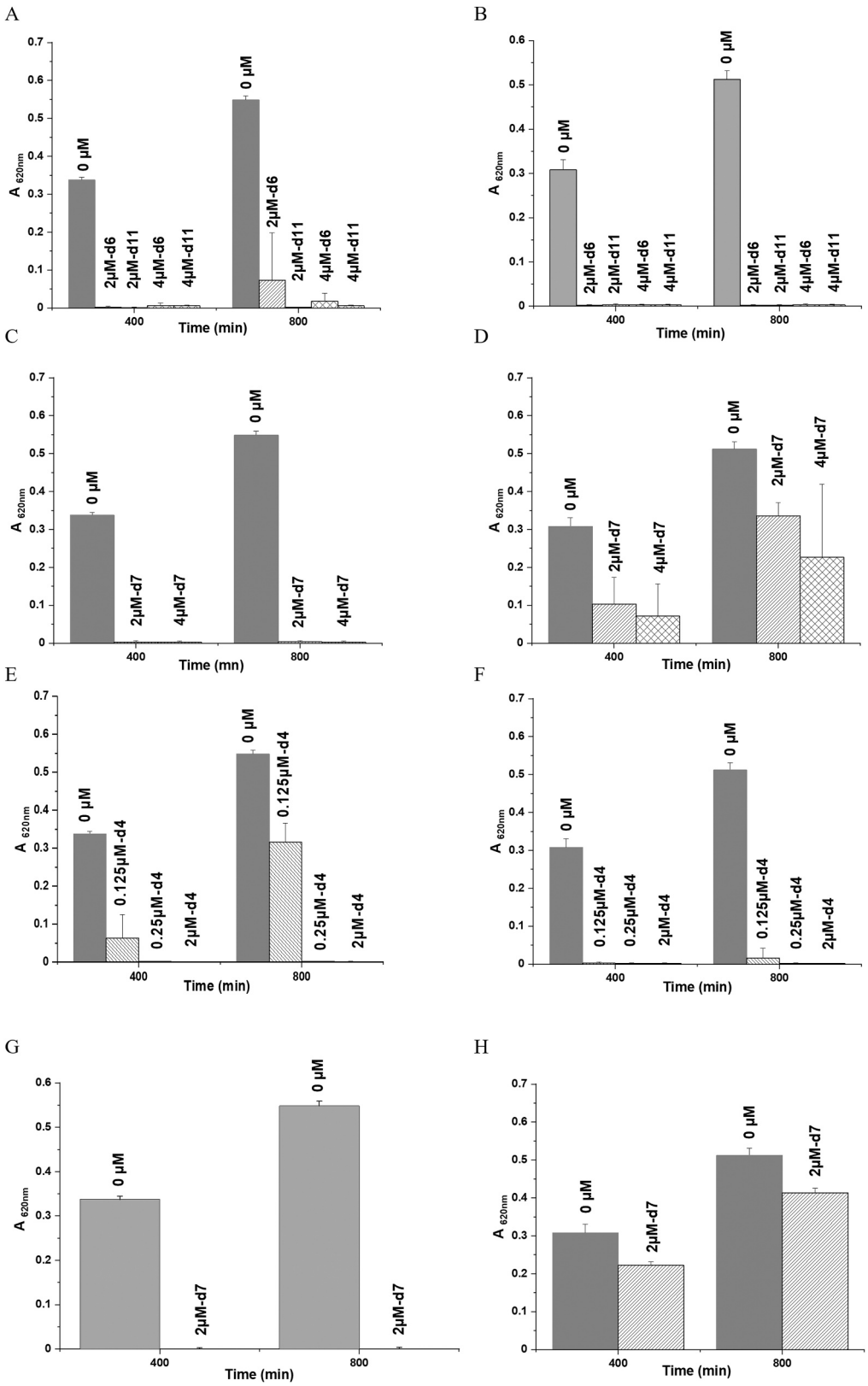

Fig. 3. Bactericidal activity and stability of the chimeras: LEGGEAEA dimer/monomer + SCN^- (A) or Cl^- (B); LEGGEAEA monomer 1 + SCN^- (C) or Cl^- (D); LGKRGAGA trimer + SCN^- (E) or Cl^- (F); LGKRGAGA dimer/monomer + SCN^- (G) or Cl^- (H); $(LEKREAEA)_2$ dimer/monomer + SCN^- (I) or Cl^- (J); $(LEKREAEA)_2$ trimer + SCN^- (K) or Cl^- (L). $A_{620\,nm}$ measurement at 400 and 800 minutes in presence of different concentrations of the chimera (as shown on each Figure) and fixed concentrations of glucose (15 mM) along with SCN^- (25 mM) or Cl^- (80 mM), at different kinetics. For all experiments, kinetics were run for 16 hours at 37°C. Kinetic experiments were repeated after several days (d) of enzyme storage at 4°C. Data at 400 and 800 minutes have been derived from the kinetic curves. Bactericidal activity was measured at 37°C and assessed in triplicate.

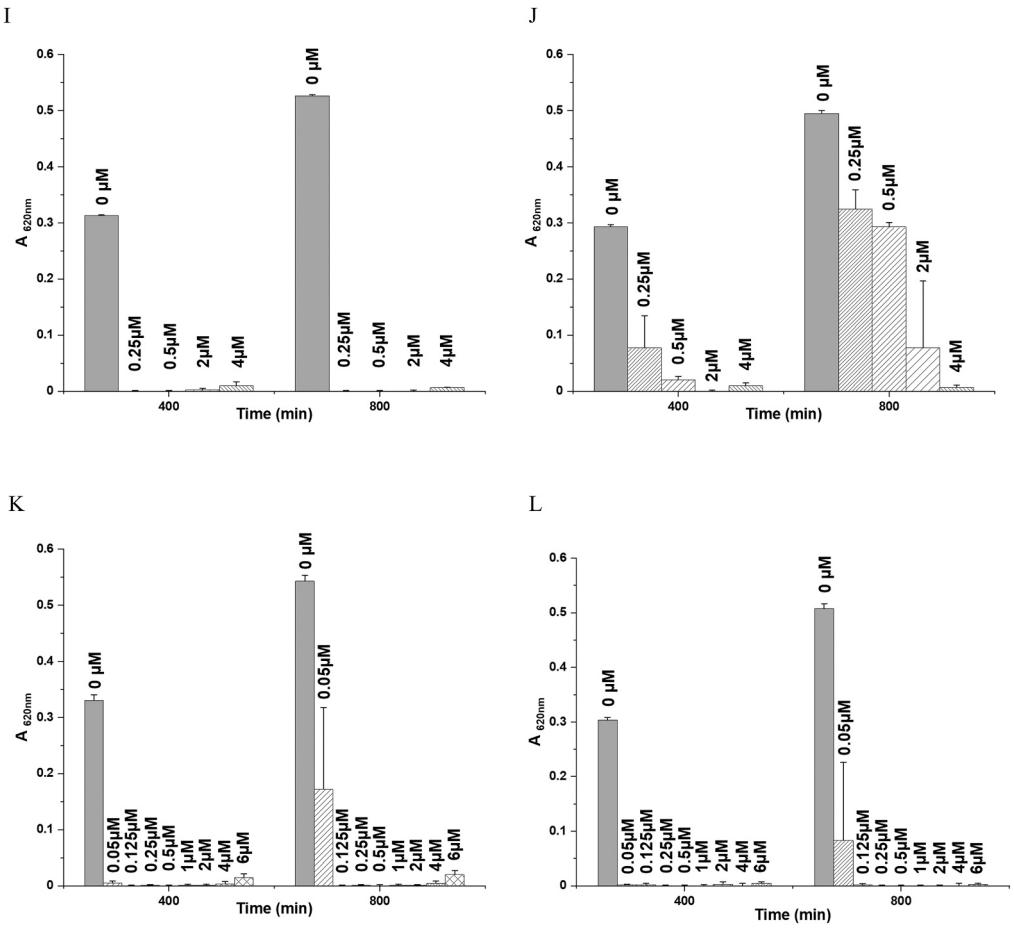

Fig. 3. (*continued*).

(Figure S12), AFM (Fig. 4 and Figure S13), or TEM (Figure S14).

Cryofracture offers the advantage of analysing the enzyme in solution. WO, the multimer and monomer, and the chimera with the LEKREAEA linker were observed by cryofracture. The results showed that the diameter of the enzyme increased with the apparent oligomeric state (Figure S12). AFM imaging enabled to compute the 2D, 3D profile and the dimension of the particles deposited on a mica surface. Chimeras with linkers LEKREAEA, LEKRPEAEA, LEKREAEALEKREAEA, LEGGEAEA, LGKRGAGA and GGGGGGGGG and were analysed (Fig. 4). As can be observed, the profiles of the chimeras are different. LEKREAEA present a ball shape (Fig. 4A) whose height varies from 0.5 to 1.7 nm (Figure S13A). Indeed, elongated hooked rod-shaped particles can be observed for LEKRPEAEA (Fig. 4B) with particle heights between 0.6 and 0.7 nm (Figure S13B). The LEKREAEALEKREAEA monomer has a more or less round shape (Fig. 4C) and particle heights between 0.4 and 0.6 nm (Figure S13C). On the other hand, the LEGGEAEA monomer, has a more oblong, rounded shapes (Fig. 4D) and heights ranging from 1.4 to 1.6 nm (Figure S13D). Finally, the LGKRGAGA trimer and GGGGGGGG dimer/monomer have rounded shapes (Figs. 4E and 4F) with heights ranging from 0.5 to 4 nm and from 1 to 8 nm respectively (Figure S13E and S13F). Although not all chimeras were analysed, by AFM these results suggested that the nature of the linker also modifies their topology. Moreover, the height of the objects observed suggests that the chimeras with LEKRPEAEA and LEKREAEALEKREAEA linkers are more spatially extensive than chimeras with LEGGEAEA linkers, which are oblong or with LEKREAEA, LGKRGAGA or GGGGGGGG linkers, which are round. Three among these four chimeras were also studied by TEM (Figure S14), they appeared round and capable of forming aggregates.

2.4.3. *Mix of oligomeric states*

Finally, in the perspective of a possible application, it seems interesting to test the efficiency of a mixture of the different oligomeric states of the LEGGEAEA chimera. As shown in Fig. 5A obtained in AFM tapping mode, enzymes with different size (diameters) were present in the sample, reflecting the presence of different oligomeric states of the chimera. Statistics on 40 particles from three different images allow to determine that 27 % of chimera have a diameter of between 20 and 35 nm with a height between 2 and 6 nm; 55 % have a diameter of between 40 and 50 nm with a height of between 2 and 6 nm and 18 % have a diameter of between 55 and 70 nm with a height of between 3 and 8 nm. Microbicidal activity was tested against the ATCC25922 strain towards SCN^- and Cl^-. The kinetic experiments presented in Fig. 5B demonstrated that cellular growth was inhibit for up to 16 hours. The Petri dish colony counting method failed to detect any surviving colonies, as shown in Fig. 5C. To highlight the advantages of the chimera over the coupled enzyme system, activity tests were performed in the presence of an increasing concentration of catalase. Catalase concentrations were chosen to be in excess of to GOx activity. The results are presented in Fig. 5D and show significantly that a higher amount of catalase was required to decrease HOCl production yields by the chimera compared with the coupled enzyme system. Keeping the two enzymes close to each other offers an advantage for HOCl production in the presence of catalase.

3. Discussion

It has been shown in the literature that enzymatic engineering makes it possible to obtain new, less expensive, enzymes that are more adapted to the research context (Ozbakir et al., 2018). It has also been shown that

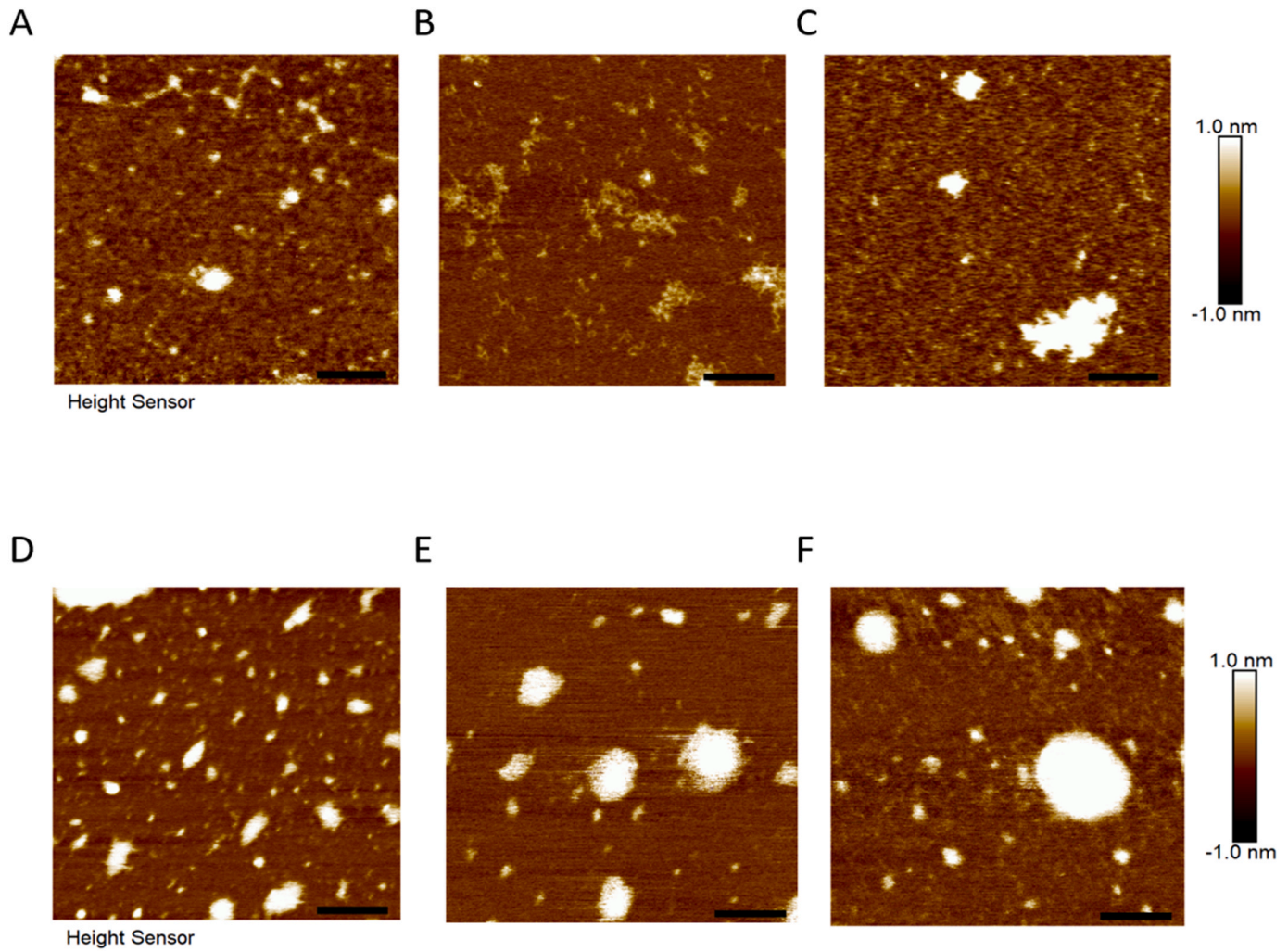

Fig. 4. AFM images in Tapping mode 2D images of**:** A) LEKREAEA; B) LEKRPEAEA mutimer; C) LEKREAEALEKREAEA dimer/monomer; D) LEGGEAEA monomer 1; E) LGKRGAGA trimer; F) GGGGGGGG dimer/monomer. Scale bars A–F: 100 nm; height range: A–F: 1 nm.

the use of a chimera is a good way of exploiting the enzymatic properties of each partner for a whole range of possible applications (Colpa et al., 2017). Furthermore, the activities of constructed chimeras can be enhanced by adding a peptide linker between the two enzymes of the chimera, and the intrinsic properties of this linker can increase the catalytic efficiency of chimeras up to 500-fold (Kummer et al., 2021). The present study has therefore provided a wealth of information on the influence of linkers on chimera activities. The addition of peptide linker, whose sequence is LEKREAEA, resulted in a trimeric form of the enzyme that was more active than the WO monomer, mainly in terms of GOx activity. To characterize this new linker (compared to the typical sequence found in the literature for the linker (Huang et al., 2021); Gran-Scheuch et al., (2021); Ceballos-Alcantarilla and Merkx, (2021)), a functional study of this 8 amino acid linker was performed. Several criteria were considered when preparing the linker library: peptide size, flexibility and the nature of the amino acids. It turned out that several oligomeric states for each chimera were possible and purified. A summary of the interest of the chimeras for their kinetic parameters shows that: i) the LEGGEAEA monomeric chimera with an anionic linker was the most active, and inhibition by excess substrates was low; ii) the LEKRPEAEA trimer with a Pro in the middle of the linker was active, and inhibition by excess substrates was low; iii) LGKRGAGA with a cationic linker was highly active but showed strong inhibition by excess substrates; iv) GGGGGGGG had low activity and was weakly inhibited and v) LEKREAEALEKREAEA with the longest linker appeared to be highly active. It appears that the presence of negative and/or positive charges on the linker plays a crucial role in optimizing the activity of the chimera. The most effective chimera had a linker that was predominantly negatively charged, while a neutral linker resulted in a decreased activity. The addition of the P seems to be essential for the stability of the chimera. For instance, microbicidal assays conducted on LEKRPEAEA after 6 months of storage at 4°C showed it retained the same activity as the fresh enzyme (data not shown). If the linker is too long, inhibition by H_2O_2 becomes more pronounced. Even tough may remain highly active and microbicide, the potential application could be limited due to substrate inhibition. The physico-chemical properties and nature of the linker significantly influence the kinetic properties and topology of the chimera. The LEKRPEAEA linker provides the clearest example, exhibiting a bent shape due to the biochemical natural properties of proline, which induces curvature and enhances rigidity. The enzymes were added to *E. coli* ATCC25922 to characterize the enzyme's microbicidal capacity. Tests were performed at 37°C in the optimal medium for the strain for 16 h. The enzymes had to be active at least 16 h at 37°C in a buffer not optimal for their stability. The results showed that enzymes without linkers were inactive against the *E. coli* strain. Enzymes with anionic or cationic linkers showed microbicidal activity with both tested substrates. Enzymes with the longest linker were highly efficient, at low enzyme concentration in slowing down the growth of *E. coli* strain. In conclusion, the presence or absence of a linker adversely affected the chimera activity and antimicrobial efficiency against *E. coli*. Activities

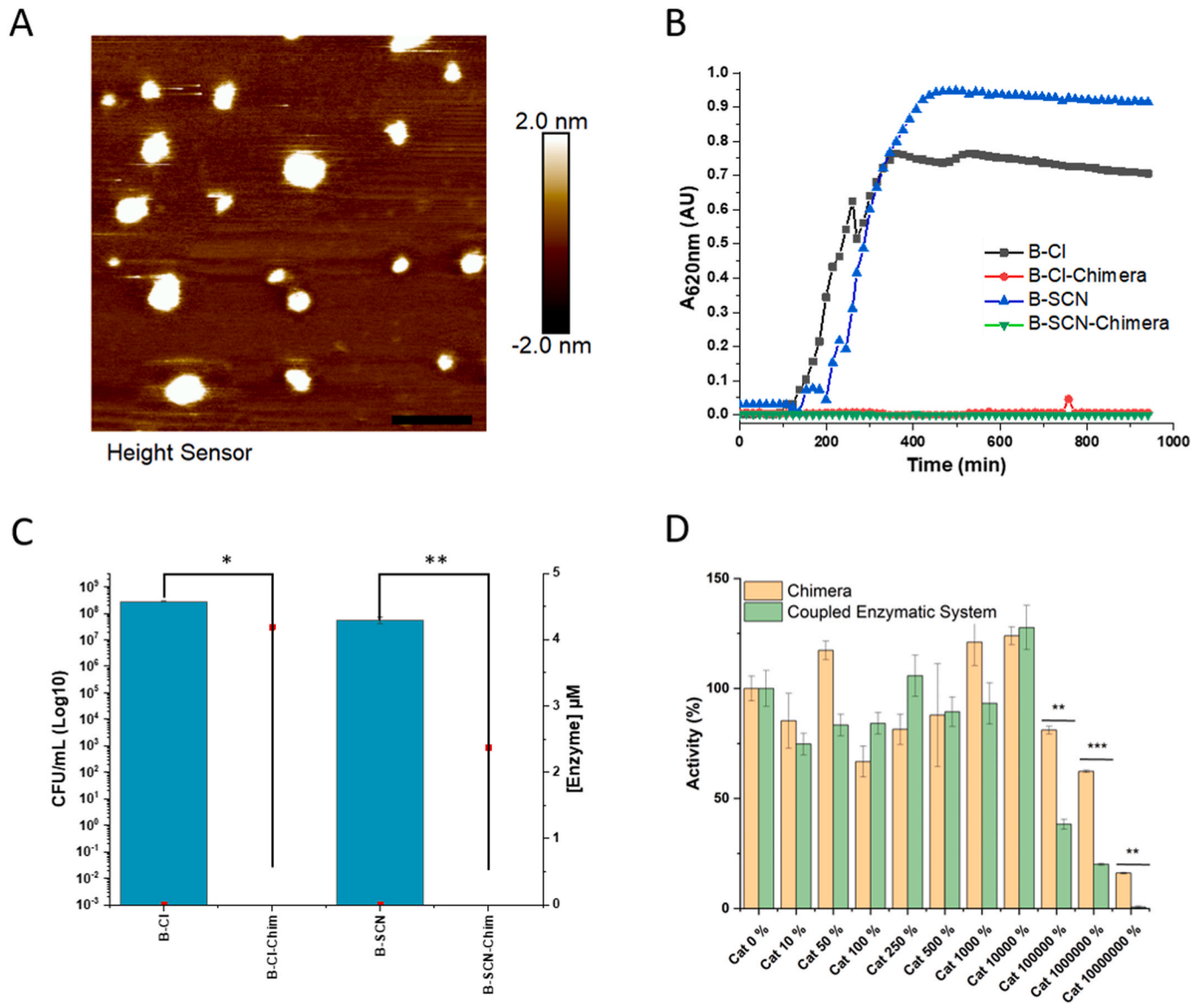

Fig. 5. Antibactericidal activity of the LEGGEAEA chimera in the presence of 5 mM of glucose with 25 mM of SCN^- or 380 mM of Cl^-. A) AFM image in Tapping mode of a mixture of several oligomeric state of LEGGEAEA; scale bar 500 nm; height range 2 nm; B) Absorbance at 620 nm measurement for a 16 h kinetic with 2.37 µM (Cl^- condition) and 4.19 µM (SCN^- condition). C) Histogram summarizing the different conditions tested in the presence of 1.10^6 Colony Forming Unit (CFU)/mL (noted B- on the *x*-axis) and in contact for 3 h with the enzyme solution at pH 7.5. We tested two different pseudo- halogenated substrates: Cl^- and SCN^- (labeled Cl and SCN respectively on the x-axis). The CFU/mL defined on the ordinate axis (in log 10) correspond to the number of surviving bacteria after one night at 37 °C in the incubator. The second ordinate axis corresponds to the concentration LEGGEAEA chimera present in the incubation solution. * means that the difference is statistically significant with a *p*-value of less than 0.05. Anova test (NaCl) p-value: 0.00663 (*) and (NaSCN) p-value: 0.01498 (**). And D) Production of HOCl of the LEGGEAEA chimera or the coupled enzymatic system composed of 300 nM of RbMPO and 25 nM of GOx in presence of increasing concentrations of catalase. * * means that the difference is statistically significant with a *p*-value of less than 0.01 and * ** means that the difference is statistically significant with a *p*-value of less than 0.001. Anova test (Cat 100000 %) p-value: 0.00356; (Cat 1000000 %) p-value: 0.00025 and (Cat 10000000 %) p-value: 0.00169.

were affected and were very low for the chimera without linker. This is certainly a misfolded protein whose stability is inferior to that of the other chimeras. Neutral linkers affected microbicidal activity with Cl^-. Insertion of a Pro could promote the correct angle between the two enzyme making up the bifunctional chimera. As shown by AFM, the chimera with Pro has a different hooked stem shape compared to the shape observed for the other chimeras. This shape could enhance stability and substrate transfer between the two active sites. The LEGGEAEA monomer has an oblong shape and was different from the LEKREAEA trimer, which has a rounded shape. The various monomeric and dimeric forms of the chimeras were deposited at pH 7.5 on a freshly cleaved sheet of highly hydrophilic mica. At this pH, the mica surface and the multimers are negatively charged, favoring solution spreading. Evaporation of the aqueous film induces capillary forces that undoubtedly generated aggregates with large lateral dimensions. However, the measured heights, ranging from 0.6 to 2.5 nm, reflect fairly well the monomer dimensions measured by SAXS (and DLS).

In the literature, AFM measurements have shown that human MPO has a diameter of 4–7 nm and a height of 4 nm (Barinov et al., 2018) and GOx from that *Aspergillus niger* has a diameter of 10–14 nm and a height of 6–8 nm (Muguruma et al., 2006). Human MPO is a dimer of heterodimer of around 150 kDa and GOx is a homodimer of around 60 kDa. Our measurements were consistent with these data. In conclusion, in this study concerning the functionality of peroxidase-oxidase chimeras, linker length, shape, charge and flexibility appear to be very important for final stability, activity and folding. Furthermore, the existence of

different oligomeric states is certainly due to glucose oxidase's natural ability to exist in dimeric form. At this stage, we cannot rule out the possibility that RbMPO exists in multimeric form, but it is likely to be in dimeric form, as shown by SAXS measurements. The mixture of chimeras is microbicidal, contains the different oligomeric forms of the enzyme and, above all, we have shown that in the presence of catalase, HOCl production resists better than in the coupled enzymatic system made up of the two stand-alone RbMPO and GOx enzymes. This last result highlights the importance of keeping the two enzymes in close proximity to each other to enhance activity by increasing the local concentration of H_2O_2 around RbMPO. Computational approaches, biochemical methods (such as BN-PAGE analysis or co-immunoprecipitation experiments between the monomeric chimera and RbMPO or GOx) or biophysical methods (such as FRET or FRAP) could be highly instructive to better understand the structure and functions of the chimeras created in this study from a fundamental point of view. The substrates specificities of the different chimeras towards Br^- and I^- could also be studied in the future and compared to other natural enzymes (Céré et al., 2023; Thapa and Agarwal, 2021; Singh et al., 2022). Detailed kinetic studies could also be performed as it has been done on natural bifunctional dimethylglycine oxidase (Basran et al., 2006). Finally, combination with other antimicrobial methods could be considered as it has been done with ultrasonic waves used in synergy with proteases (Oulahal-Lagsir et al., 2003). More generally, knowledge of high-resolution structure of the chimera, i.e. by cryo-electron microscopy, would provide molecular-level information on the structure-function relationship of these artificial bifunctional enzymes. Recent studies have focused on the determination of the 3D structure of natural bifunctional multidomain enzymes (Mycroft-West et al., 2024; Leo et al., 2024).

4. Material and Methods

4.1. Construction of the chimera by fusion PCR

Amplification of the GOx_{penag} ORF in pPICZα (Invitrogen™) (Courjean and Mano, 2011) was achieved by introducing two restriction sites from NEB Biolabs: *Nde*I and *Xho*I (oligonucleotide used: 5'-aaaaaaaaaaaaaaacatatgtacctgcctgcccaacagattgatg-3' and 3'-agctggc ggccgccgcggctcgagctaggcacttttggcatagtcatcc-5'). The amplified DNA (with PCR apparatus Biorad T100) was then digested by the two previously introduced restriction sites and the GOx_{penag} ORF was ligated into a plasmid pET21a(+)DNA-Novagen (digested with *Nde*I and *Xho*I). On the other hand, the vector pEt21aRbMPO-6His (Céré et al., 2023) was digested with *Xho*I and the pET21aGOx_{penag} with *Nde*I. The two linearized vectors were used as megaprimers for the following two primers: "RbMPO in 3'" 5'-agcgaggacgataaaatccaggccgcgaattctttccgc-3' and "GOx_{penag} in 5'" 5'-tacctgcctgcccaacagattgatgtccagtctag-3'. The PCR product was digested with *Dpn*I from Takara for 2 h at 37°C, followed by DNA purification. A final ligation step precedes the transformation of the new construct into *DH5*α (Hanahan, 1983). To check whether the chimeric construct is correct, clones were tested by colony PCR using two oligonucleotides from Sigma-Aldrich that will amplify the fusion zone: "GOx65rc" 5'-ggtgccaaagatttctccataagcatttg-3' and "RbMPOH407A" 5'-ccgccgcgtttcggttgggggcgagcacgcttcgtg-3'. The plasmid pET21aRbMPO-GOx was obtained.

4.2. Construction of the chimera by sub-cloning

The plasmid pPiczαGOx_{penag} (Courjean and Mano, 2011) was digested by the restriction enzyme *Xho*I present at two sites on either side of the enzyme ORF. On the other hand, the plasmid pET21aRbMPO-6His was digested with *Xho*I, which was located at the 3' of the enzyme ORF just before the 6His tag coding sequence. The linearized plasmid undergoes ligation with the ORF of GOx_{penag} to obtain the final chimeric construction. As with the fusion technique, the construction was verified after transformation in *DH5*α bacteria by colony PCR with GOx 65rc and RbMPOH407A oligonucleotides. Plasmid pET21aRbMPO-LEKREAEA-GOx was obtained.

4.3. Linker modifications by genetic engineering

Either Quick Change kit from Stratagene or Q5 site directed mutagenesis kit from NEB Biolabs were used to modified chimeras. pET21aRbMPO-GOx without linker was used as template to add a sequence coding 8 Gly or LGKRGAGA. pET21aRbMPO-LEKREAEA-GOx was used as template 1) to insert a sequence coding LEKREAEA to obtain a linker coding LEKREAEALEKREAEA or 2) to mutate the sequence coding linker into LEGGEAEA or 3) to insert a sequence coding a Pro to obtain LEKRPEAEA linker. 5 plasmidic constructions were obtained with the modified linker. Oligonucleotides used to perform these experiments are described in Table S5.

4.4. Production and purification of the chimera

The pET21aWTRbMPO-GOx_{penag} was transformed in *E.coli* BL21Star (DE3) pLysS and bacterial clones were grown on LB agar nutrient medium containing ampicillin and chloramphenicol. 1 L was incubated with 10 mL of a pre-culture from the previous day, and $A_{600\ nm}$ was measured up to the exponential phase of bacterial growth (0.5–0.8). Induction with 500 μM IPTG was used to trigger transcription and translation of the chimera. After 24 hours at 22°C the cultures were pelleted. Bacteria were crushed twice (TS2 0.75 kW Serie Bench Top, Constant systems Ltd., Daventry, United-Kingdom) at 2200 bar and at 4°C and the bacterial pellet was washed with a solution of 2 M urea, 50 mM Tris, 5.5 mM $CaCl_2$ pH 7.5. The chimera 142088.88 Da in size, was produced in the bacterial inclusion bodies. Treatment of the pellet with a solution of 8 M urea, 50 mM Tris, 5.5 mM $CaCl_2$ pH 7.5 during 4 hours at 4°C was then necessary to resolubilize all proteins. The supernatant recovered after centrifugation was poured into a reconstitution solution (Tris 20 mM pH 7.5, 5.5 mM $CaCl_2$, 5 μM hemin, 200 μM FAD, 1 mM oxidised glutathione, 1 mM reduced glutathione and 10 % v/v glycerol) for 5, 8 or 15 days. The mixture was concentrated first with a concentration cassette (Sartorius PES Cassettes Vivaflow 200 with a 30 kDa cut off) and then with a 30 kDa amicon (Merck-Millipore amicon Ultra-15, PLHK, membrane Ultracel-PL) to obtain a volume of less than 13 mL. The protein solution was injected onto a size exclusion chromatography (Hiload 26/600 200pn Cytiva: fractionation range 10000–600000 Da). After isocratic elution (50 mM Tris, 5.5 mM $CaCl_2$ pH 7.5), the peak(s) containing the chimera were concentrated. The column was calibrated with a Biorad gel filtration standard.

4.5. UV spectra

The UV spectrum of the chimeras was determined using a spectrophotometer Cary 100 system from Varian, Inc. (Palo Alto, CA), equipped with a Peltier thermostable multicell holder that scanned the protein sample (diluted at 2.5 μM) from 800 to 200 nm. The theoretical epsilon at 280 nm of chimera, RbMPO and GOx are respectively of 144,285, 49,850 and 96,845 $M^{-1}.cm^{-1}$ and was determined by using expasy protparam tools (Wilkins et al., 1999) and Beer Lambert's law were used to determine the concentration of pure enzyme after purification.

4.6. SDS-PAGE

Mini-PROTEAN® Precast Gels (Bio-rad) were used. These gels were characterised by a gradient of 4–15 % acrylamide. The analysed protein samples were homogenised with Filler Blue 4X (containing SDS and β-mercaptoethanol) and then heated to 95°C for 5 minutes. Denaturing migration buffer (SDS) and 35 mA amperage per gel were used to migrate proteins according to their molecular weight. After migration, the gel was stained for 3 hours in a Coomassie blue solution and then

underwent successive fading steps in a 10 % acetic acid 30 % ethanol solution.

4.7. Small angle X-rays scattering (SAXS)

SAXS measurements were carried out on the LEGGEAEA chimera, whose individual oligomers were freshly separated on an S200 column, using a XEUSS 2.0 setup (XENOCS, Grenoble, France). It uses a sealed-tube microfocused Cu K-alpha source with a wavelength of 1.54 Å. Experiments were carried out with a 0.55 × 0.3 mm collimated beam. The distance between sample and detector, calibrated with a silver behenate standard, was set at 1.85 m to obtain an accessible Q range from 0.005 Å-11–0.21 Å-1. The various enzyme solutions were loaded into thin quartz capillaries (1.5 mm optical path, WJM-Glas/Müller GmbH, Germany) and the signal collected for 3 hours to obtain good statistics over the whole Q range. The respective capillary, solvent and dark scattering were subtracted using standard protocols. Data were normalized to absolute units in cm^{-1}.

The Mw of the various enzymes studied in this work were determined using a standard protein, lysozyme, according to the following equation (Mylonas and Svergun, 2007).

$$M_w^{enzyme} = \frac{M_w(Lyso)}{I(0)^{Lyso}/C_{Lyso}} I(0)^{enzyme}/C_{enzyme} \quad (1)$$

where $I(0)^{lyso}$ and $I(0)^{enzyme}$ are the scattering intensities at zero angle of the lysozyme and the studied enzyme, respectively, M_w^{Lyso} and M_w^{enzyme} are the corresponding molecular masses and c_{lyso} and c_{enzymz} are the concentrations. SasView software (https://www.sasview.org/) was used to process and fit the data.

4.8. Atomic force microscopy (AFM)

The enzymes were characterized in air by AFM in Tapping mode using Bruker Dimension Icon AFM instrument with a Tap 300Al-G Budget Sensors tip. A drop of solution containing the chimeric enzymes at 0.01 mg/mL or the mixture of LEGGEAEA at 0.001 mg/mL was deposited on a freshly cleaved mica substrate and allowed to evaporate at room temperature for 48 h in a laminar hood. Raw images were then processed and analyzed using Nanoscope Analysis software.

4.9. GOx_{penag} activity

The D-Gluconic acid/D-Glucono-δ-lactone kit from Megazyme were used. The day before, a solution containing 5 μM of chimera, 250 mM glucose and 50 mM NaPi pH6 was incubated at 37°C. The next day, 15.7 μL of this solution was taken and the activity of the GOx_{penag} in the chimera was measured at 340 nm, corresponding to the wavelength of the kit's final product: NADPH. The concentration of D-gluconic acid produced by the chimera after one night of reaction was calculated using the following relationship:

$$[D-gluconic\ acid](g/L) = \frac{V * MW}{\varepsilon_{NADPH} * v} \Delta A_{340nm} \quad (2)$$

Where $\varepsilon_{NADPH} = 6300\ M^{-1}.cm^{-1}$ is the extinction coefficient of NADPH at 340 nm; V corresponds to the final volume; MW corresponds to the molecular weight of D-gluconic acid and is 196.1 g/mol; v corresponds to the sample volume and $\Delta A_{340\,nm}$ corresponds to the absorbance variation at 340 nm measured during the test included in the kit.

4.10. Chlorination activity

The fluorescent probe APF from Sigma-Aldrich ($\lambda_{excitation} = 485$ nm and $\lambda_{emission} = 525$ nm) was used to measure the HOCl production by the chimera. Three series were performed, the first being a glucose series (0,1, 2, 3, 4, 5, 6, 8, 10, 15, 20 mM) with a fixed concentration of enzyme, 1 μM and NaCl (NaCl BioXtra from Sigma-Aldrich), 20 mM. The second series was run with increasing concentrations of NaCl (0, 10, 20, 50, 100, 250, 500, 750 μM and 1 mM) with the same enzyme concentration as above and a fixed glucose concentration of 20 mM. The final series was an H_2O_2 range with the following concentrations tested: 0, 0.01, 0.02, 0.05, 0.079, 0.1, 0.25, 0.5, 0.75, 1, 2, 4, 6, 8, 10, 20, 40, 60, 80, 100, 200, 500 mM with 1 μM of chimera and 20 mM of NaCl. For all experiments 10 μM APF was used in each assay with 50 mM NaPi buffer pH7.5 QSP 20 μL (384-well plate). Each measurement was performed in triplicate. To analyse the data, 3 equations have been used:

$$k_{ss} = \frac{k_{cat} * [S]}{K_M + [S]} \quad (3)$$

$$k_{ss} = \frac{k_{cat} * [S]}{K_M + [S] * (1 + \frac{[S]}{K_i})} \quad (4)$$

$$k_{ss} = \quad k_2 * [S] \quad (5)$$

k_{ss} is the steady-state rate constant; S is the substrate of interest (either glucose, NaCl or H_2O_2); K_M the Michaelis constant of the substrate of interest; K_I is the inhibition constant of the substrate of interest; k_{cat} is the catalytic rate constant and k_2, the slope of the straight line through 0.

4.11. Antimicrobial activity

The glycerol stock of *E. coli* ATCC 25922 strain was deposited onto a Petri dish containing TSB agar medium (from Fischer Scientific) for 16 hours at 37°C. 10 mL of TSB medium (from Fischer Scientific) was inoculated with an isolated bacterial colony and the pre-culture was agitated at 190 rpm and 37°C overnight. 25 mL of TSB medium were inoculated with the volume of pre-culture necessary to obtain an $A_{620\,nm}$ of 0.09 in a spectrophotometer (Ultrospec 10, Biochrom). Once this had been reached the exponential phase, a bacterial dilution of 10 mL (in TSB) was performed to obtain a bacterial quantity of 2.10^6 Colony Forming Unit (CFU)/mL with the correspondence of 1 $A_{620\,nm}$ to 1.10^8 CFU/mL. The microbicidal tests were performed in 96-well microplates (Greiner Bio-One™, Cellstar™ μclear™, white, flat-bottom) in a final volume of 100 μL per well, with each experimental condition in triplicate. In each well, 50 μL of bacteria were plated to be at 1.10^6 CFU/mL in all conditions. $A_{620\,nm}$ was measured with a Wallac Victor2 1420 microplate reader or a SpectraMax® Paradigm® (Molecular Devices), every 15 min for 16 h with shaking before each reading as well as a thermostatic atmosphere at 37°C. Concerning the microbicidal assay with the mixture of LEGGEAEA for mode kinetic assay, bactericidal tests were performed in 48-well microplates under a final volume of 500 μL, with 10^6 CFU/mL. The plate cover was treated with 0.05 % Triton X-100 and 20 % ethanol to prevent condensation and, consequently, errors in reading the wells by the instrument. The solution was allowed to act on the lid for 10 min, then removed and dried under a class II biological safety cabinet. Each tested condition was performed in triplicate, and each experiment was performed three times. The kinetics was set to 16 h with a measurement at 620 nm every 10 s, in a microplate reader (SpectraMaxID3) thermostated at 37°C [shaking duration: 10.0 s; shaking speed: medium; shaking type: orbital]. For all these experiments, a substrate such as Glucose, NaSCN or NaCl was at fixed concentrations of 16 mM, 25 mM and 380 mM respectively (glucose present in culture media).

For the Petri dish assay, after 3 h of the above-mentioned 16 h incubation, we made several dilutions (10^{-1} to 10^{-6}) with 100 μL of each microplate cells in 1 mL, then spread on a Petri dish containing TSB agar medium and placed at 37°C overnight. The next day, the colonies were counted, and the number of CFU/mL was calculated using the formula below: CFU/mL = Nbcolony * 10 / dilution. The concentrations of LEKREAEA chimera used were 2.37 μM in NaCl condition and 4.19 μM in NaSCN condition.

4.12. Catalase effect

Sigma-Aldrich's APF fluorescent probe ($\lambda_{excitation}$ = 485 nm and $\lambda_{emission}$ = 525 nm) was used to measure the HOCl production by 1 μM chimera or by the coupled enzymatic system composed of 300 nM of RbMPO and 25 nM of GOx, which produced the same quantity of H_2O_2 than 1 μM of chimera. Standard activity assays were performed with 10 μM APF, 500 mM NaCl and 20 mM of glucose in 50 mM sodium phosphate buffer at pH 7.5 and 37°C. Different concentrations of catalase from Sigma-Aldrich (lyophilized powder, 2000–5000 units/mg protein) were added to the assay. The concentrations of catalase used were 0, 0.494, 2.47, 4.94, 12.3, 24.7, 49.4, 494, 4940, 49400 and 494000 μg/L where these concentrations correspond respectively to 0, 10, 50, 100, 250, 500, 1000, 10000, 100000, 1000000 or 10000000 times the catalytic activity of the GOx alone or inside the chimera.

4.13. Prediction of structures

AlphaFold 3, developed by DeepMind, is an AI system that ha revolutionized protein structure prediction. Using AlphaFold integrates deep learning, particularly convolutional neural networks (Abramson et al., 2024). AlphaFold 3, we were able to predict the 3D structures of our LEGGEAEA chimera and its various oligomeric states by adding the primary sequence into the online software for two repeats (dimer) and three repeats (trimer). The models were validated based on prediction scores: pTM > 0.5 for the monomer model, pTM > 0.4 and ipTM > 0.3 for the dimer and trimer models. The resulting models obtained were analysed using the Pymol software by superimposing the known structure of the GOx onto that of the monomer chimera. This double superimposition was then applied to each model to identify which best preserved the catalytic domains of the chimera. The models that met all these criteria were then selected, and the polar interactions at the multimerization interface were further analysed.

Author Contribution

CSC supervised, designed and coordinated the work. CSC, CC, PKY and JPC wrote the manuscript. CSC and CC performed genetic engineering experiments. CSC and CC have developed the process of production and purification of the enzymes and developed activity assays. CC and PKY produced and purify the chimeras and biochemically tested them. BD has designed and done microbicidal assays. GP supervised the AFM analyses and GP and PKY performed AFM. IL supervised TEM analyses and IL and PKY performed TEM. JPC performed SAXS experiments at CRPP and AT, PKY and CSC performed preliminary SAXS assays at Synchrotron SOLEIL. PKY performed prediction of oligomer structures. CSC, CC, BD, PKY, GP, JPC and IL analyzed results. JPC proofreading and editing the text. ZI and LR helped to monitor the concentration of H_2O_2 around the chimera. VS and XL participate to scientific discussion and orientation. The manuscript was written with contributions of all authors. All authors have given their approval to the final version of the manuscript.

Funding sources

N°ANR-18-CE19–0028–01.

CRediT authorship contribution statement

Lafarge Xavier: Methodology, Investigation, Funding acquisition. **Chapel Jean-Paul:** Writing – review & editing, Writing – original draft, Methodology, Investigation, Funding acquisition, Formal analysis, Data curation. **Stines-Chaumeil Claire:** Writing – review & editing, Writing – original draft, Validation, Supervision, Project administration, Methodology, Investigation, Funding acquisition, Formal analysis, Data curation, Conceptualization. **Céré Claire:** Writing – original draft, Methodology, Investigation, Formal analysis, Data curation. **Kenfack Ymbe Parfait:** Data curation, Formal analysis, Investigation, Writing – original draft. **Rodriguez Laura:** Methodology, Investigation, Formal analysis, Data curation. **Ivanovic Zoran:** Methodology, Investigation. **Schmitt Véronique:** Methodology, Investigation, Funding acquisition. **Delord Brigitte:** Writing – original draft, Methodology, Investigation, Formal analysis, Data curation, Conceptualization. **Pecastaings Gilles:** Supervision, Methodology, Investigation, Formal analysis, Data curation. **Ly Isabelle:** Supervision, Methodology, Investigation, Formal analysis, Data curation. **Thureau Aurélien:** Methodology, Investigation.

Declaration of Competing Interest

The authors declare the following financial interests/personal relationships which may be considered as potential competing interests. Stines-Chaumeil, Delord and Céré have patent #EP22306877 / PCT/EP2023/08555 pending to University of Bordeaux / CNRS. If there are other authors, they declare that they have no known competing financial interests or personal relationships that could have appeared to influence the work reported in this paper

Acknowledgments

The work was supported by the ANR project N°ANR-18-CE19–0028–01: Microbicidal enzyme. Claire Céré is grateful to the ANR for the PhD grant. Parfait Wilfried Kenfack Ymbe is grateful for ANR support and for French Ministry of Research and Education for PhD grant.

Patent

European patent number EP22306877 and PCT/EP2023/085555 "Artificial bifunctional enzyme and applications thereof" 2022 Inventors: Stines-Chaumeil Claire, Céré Claire and Delord Brigitte. Deposited by University of Bordeaux and CNRS.

Uniprot Code

Myeloperoxidase from *Rhodopirellula baltica*: F2AVE1
Glucose oxidase from *Penicillium amagasakiense*: P81156

Appendix A. Supporting information

Supplementary data associated with this article can be found in the online version at doi:10.1016/j.jbiotec.2025.01.018.

Data availability

Data will be made available on request.

References

Aalbers, F.S., Fraaije, M.W., 2019. Enzyme fusions in biocatalysis: coupling reactions by pairing enzymes. Chembiochem 20 (1), 20–28. https://doi.org/10.1002/cbic.201800394.

Abramson, J., et al., 2024. Accurate structure prediction of biomolecular interactions with AlphaFold 3. Nature. https://doi.org/10.1038/s41586-024-07487-w.

Andrews, P.C., Krinsky, N.I., 1981. The reductive cleavage of myeloperoxidase in half, producing enzymically active hemi-myeloperoxidase. J. Biol. Chem. 256 (9), 4211–4218.

Arai, R., 2021. Chapter Eight - Design of helical linkers for fusion proteins and protein-based nanostructures. In: Merkx, M. (Ed.), Methods in Enzymology. Academic Press, pp. 209–230.

Arana-Pena, S., et al., 2021. Enzyme co-immobilization: Always the biocatalyst designers' choice…or not? Biotechnol. Adv. 51, 107584. https://doi.org/10.1016/j.biotechadv.2020.107584.

Barinov, N.A., et al., 2018. High-resolution atomic force microscopy visualization of metalloproteins and their complexes. Biochim Biophys. Acta Gen. Subj. 1862 (12), 2862–2868. https://doi.org/10.1016/j.bbagen.2018.09.008.

Basran, J., et al., 2006. Mechanism of FAD reduction and role of active site residues His-225 and Tyr-259 in arthrobacter globiformis dimethylglycine oxidase: analysis of mutant structure and catalytic function. Biochemistry 45 (37), 11151–11161. https://doi.org/10.1021/bi061094d.
Bauer, G., 2018. HOCl and the control of oncogenesis. J. Inorg. Biochem 179, 10–23. https://doi.org/10.1016/j.jinorgbio.2017.11.005.
Bülow, L., Ljungcrantz, P., Mosbach, K., 1985. Preparation of a soluble bifunctional enzyme by gene fusion. Bio/Technol. 3 (9), 821–823. https://doi.org/10.1038/nbt0985-821.
Cameron, P., et al., 2019. Harnessing type I CRISPR-Cas systems for genome engineering in human cells. Nat. Biotechnol. 37 (12), 1471–1477. https://doi.org/10.1038/s41587-019-0310-0.
Cao, Z., Cheng, G., 2022. Recombinant myeloperoxidase as a new class of antimicrobial agents. Microbiol Spectr. 10 (1), e0052221. https://doi.org/10.1128/spectrum.00522-21.
Ceballos-Alcantarilla, E., Merkx, M., 2021. Chapter One - understanding and applications of Ser/Gly linkers in protein engineering. In: Merkx, M. (Ed.), Methods in Enzymology. Academic Press, pp. 1–22.
Cegolon, L., et al., 2014. In vitro antiviral activity of hypothiocyanite against A/H1N1/2009 pandemic influenza virus. Int J. Hyg. Environ. Health 217 (1), 17–22. https://doi.org/10.1016/j.ijheh.2013.03.001.
Cegolon, L., 2020. Investigating hypothiocyanite against SARS-CoV-2. Int J. Hyg. Environ. Health 227, 113520. https://doi.org/10.1016/j.ijheh.2020.113520.
Céré, C., et al., 2023. A bacterial myeloperoxidase with antimicrobial properties. BioTech 12. https://doi.org/10.3390/biotech12020033.
Chen, X., Zaro, J.L., Shen, W.C., 2013. Fusion protein linkers: property, design and functionality. Adv. Drug Deliv. Rev. 65 (10), 1357–1369. https://doi.org/10.1016/j.addr.2012.09.039.
Chochola, J., et al., 1994. Virucidal effect of myeloperoxidase on human immunodeficiency virus type 1-infected T cells. Antimicrob. Agents Chemother. 38 (5), 969–972. https://doi.org/10.1128/AAC.38.5.969.
Colpa, D.I., et al., 2017. Creating Oxidase-Peroxidase Fusion Enzymes as a Toolbox for Cascade Reactions. Chembiochem 18 (22), 2226–2230. https://doi.org/10.1002/cbic.201700478.
Courjean, O., et al., *Effect of Degree of Glycosylation on Charge of Glucose Oxidase and Redox Hydrogel Catalytic Efficiency*. 2010. **11**(13): p. 2795-2797.DOI: https://doi.org/10.1002/cphc.201000178.
Courjean, O., Mano, N., 2011. Recombinant glucose oxidase from Penicillium amagasakiense for efficient bioelectrochemical applications in physiological conditions. J. Biotechnol. 151 (1), 122–129. https://doi.org/10.1016/j.jbiotec.2010.10.077.
El Messaoudi, K., et al., 2002. Human recombinant myeloperoxidase antiviral activity on cytomegalovirus. J. Med Virol. 66 (2), 218–223.
Ferraz, C.A., et al., 2021. Isopentenol utilization pathway for the production of linalool in Escherichia coli using an improved bacterial linalool/nerolidol synthase. Chembiochem 22 (13), 2325–2334. https://doi.org/10.1002/cbic.202100110.
Gran-Scheuch, A., et al., 2021. Chapter Five - Optimizing the linker length for fusing an alcohol dehydrogenase with a cyclohexanone monooxygenase. In: Merkx, M. (Ed.), Methods in Enzymology. Academic Press, pp. 107–143.
Hanahan, D., 1983. Studies on transformation of Escherichia coli with plasmids. J. Mol. Biol. 166 (4), 557–580. https://doi.org/10.1016/S0022-2836(83)80284-8.
Huang, Z., Zhang, C., Xing, X.-H., 2021. Chapter Two - Design and construction of chimeric linker library with controllable flexibilities for precision protein engineering. In: Merkx, M. (Ed.), Methods in Enzymology. Academic Press, pp. 23–49.
Iyengar, A.R.S., et al., 2019. Protein chimerization: a new frontier for engineering protein therapeutics with improved pharmacokinetics. J. Pharmacol. Exp. Ther. 370 (3), 703. https://doi.org/10.1124/jpet.119.257063.
Ji, S., et al., 2023. Computational design and structure dynamics analysis of bifunctional chimera of endoxylanase from Clostridium thermocellum and xylosidase from Bacteroides ovatus. 3 Biotech 13 (2), 59. https://doi.org/10.1007/s13205-023-03482-6.
Jiao, J., et al., 2022. A bifunctional enzyme of legionella that distinctly regulates phosphoribosyl ubiquitination of the side family effectors. J. Transl. Int Med 10 (2), 86–88. https://doi.org/10.2478/jtim-2022-0014.
Khera, H.K., Singh, S.K., Singh, S., 2019. Chorismate synthase from malaria parasites is bifunctional enzyme. Mol. Biochem Parasitol. 233, 111202. https://doi.org/10.1016/j.molbiopara.2019.111202.
Kummer, M.J., et al., 2021. Substrate channeling by a rationally designed fusion protein in a biocatalytic cascade. JACS Au 1 (8), 1187–1197. https://doi.org/10.1021/jacsau.1c00180.
Kuzmak, A., et al., 2019. Can enzyme proximity accelerate cascade reactions? Sci. Rep. 9 (1), 455. https://doi.org/10.1038/s41598-018-37034-3.
Leo, G., et al., 2024. Structural insights into the bifunctional enzyme human FAD synthase. Structure. https://doi.org/10.1016/j.str.2024.04.006.
Lu, J., et al., 2016. The development of leucine dehydrogenase and formate dehydrogenase bifunctional enzyme cascade improves the biosynthsis of L-tert-Leucine. Appl. Biochem Biotechnol. 180 (6), 1180–1195. https://doi.org/10.1007/s12010-016-2160-2.
Lu, P., Feng, M.G., 2008. Bifunctional enhancement of a beta-glucanase-xylanase fusion enzyme by optimization of peptide linkers. Appl. Microbiol Biotechnol. 79 (4), 579–587. https://doi.org/10.1007/s00253-008-1468-4.
Manjasetty, B.A., et al., 2001. Crystallization and preliminary X-ray analysis of dmpFG-encoded 4-hydroxy-2-ketovalerate aldolase–aldehyde dehydrogenase (acylating) from Pseudomonas sp. strain CF600. Acta Crystallogr D. Biol. Crystallogr 57 (Pt 4), 582–585. https://doi.org/10.1107/s0907444901000439.
Manjasetty, B.A., Powlowski, J., Vrielink, A., 2003. Crystal structure of a bifunctional aldolase-dehydrogenase: sequestering a reactive and volatile intermediate. Proc. Natl. Acad. Sci. USA 100 (12), 6992–6997. https://doi.org/10.1073/pnas.1236794100.
Muguruma, H., et al., 2006. Adsorption of glucose oxidase onto plasma-polymerized film characterized by atomic force microscopy, quartz crystal microbalance, and electrochemical measurement. J. Phys. Chem. B 110 (51), 26033–26039. https://doi.org/10.1021/jp063755m.
Mycroft-West, C.J., et al., 2024. Structural and mechanistic characterization of bifunctional heparan sulfate N-deacetylase-N-sulfotransferase 1. Nat. Commun. 15 (1), 1326. https://doi.org/10.1038/s41467-024-45419-4.
Mylonas, E., Svergun, D.I., 2007. Accuracy of molecular mass determination of proteins in solution by small-angle X-ray scattering. J. Appl. Crystallogr. 40 (s1), s245–s249. https://doi.org/10.1107/S002188980700252X.
Oulahal-Lagsir, N., et al., 2003. Escherichia coli-milk" biofilm removal from stainless steel surfaces: synergism between ultrasonic waves and enzymes. Biofouling 19 (3), 159–168. https://doi.org/10.1080/08927014.2003.10382978.
Ozbakir, H.F., Garcia, K.E., Banta, S., 2018. Creation of a formate: malate oxidoreductase by fusion of dehydrogenase enzymes with PEGylated cofactor swing arms. Protein Eng. Des. Sel. 31 (4), 103–108. https://doi.org/10.1093/protein/gzy005.
Permana, D., et al., 2021. Strategies for making multimeric and polymeric bifunctional protein conjugates and their applications as bioanalytical tools. Anal. Sci. 37 (3), 425–437. https://doi.org/10.2116/analsci.20SCR07.
Persoon, I.F., et al., 2012. Effect of vanadium chloroperoxidase on Enterococcus faecalis biofilms. J. Endod. 38 (1), 72–74. https://doi.org/10.1016/j.joen.2011.09.003.
Persoon, I.F., et al., 2013. Antimicrobial effect of a modified vanadium chloroperoxidase on Enterococcus faecalis biofilms at root canal pH. J. Endod. 39 (8), 1035–1038. https://doi.org/10.1016/j.joen.2013.04.038.
Phan-Xuan, T., et al., 2020. Hydration-induced structural changes in the solid state of protein: a SAXS/WAXS study on lysozyme. Mol. Pharm. 17 (9), 3246–3258. https://doi.org/10.1021/acs.molpharmaceut.0c00351.
Pony, P., et al., 2020. Filamentation of the bacterial bi-functional alcohol/aldehyde dehydrogenase AdhE is essential for substrate channeling and enzymatic regulation. Nat. Commun. 11 (1), 1426. https://doi.org/10.1038/s41467-020-15214-y.
Rabeharindranto, H., et al., 2019. Enzyme-fusion strategies for redirecting and improving carotenoid synthesis in S. cerevisiae. Metab. Eng. Commun. 8, e00086. https://doi.org/10.1016/j.mec.2019.e00086.
Receveur-Brechot, V., Durand, D., 2012. How random are intrinsically disordered proteins? A small angle scattering perspective. Curr. Protein Pept. Sci. 13 (1), 55–75. https://doi.org/10.2174/138920312799277901.
Reddy Chichili, V.P., Kumar, V., Sivaraman, J., 2013. Linkers in the structural biology of protein-protein interactions. Protein Sci. 22 (2), 153–167. https://doi.org/10.1002/pro.2206.
Schürmann, N., et al., 2017. Myeloperoxidase targets oxidative host attacks to Salmonella and prevents collateral tissue damage. Nat. Microbiol. 2 (4), 16268. https://doi.org/10.1038/nmicrobiol.2016.268.
Singh, P.K., et al., 2022. Structural evidence of the oxidation of iodide ion into hyper-reactive hypoiodite ion by mammalian heme lactoperoxidase. Protein Sci. 31 (2), 384–395. https://doi.org/10.1002/pro.4230.
Smith, N.E., et al., 2014. Binding and channeling of alternative substrates in the enzyme DmpFG: a molecular dynamics study. Biophys. J. 106 (8), 1681–1690. https://doi.org/10.1016/j.bpj.2014.03.013.
Thapa, H.R., Agarwal, V., 2021. Obligate Brominating Enzymes Underlie Bromoform Production by Marine Cyanobacteria. J. Phycol. 57 (4), 1131–1139. https://doi.org/10.1111/jpy.13142.
Wang, R., Sun, F., 2021. Chapter Eleven - The Spy that links: Creation of nonlinear protein architectures and materials using SpyTag/SpyCatcher chemistry. In: Merkx, M. (Ed.), Methods in Enzymology. Academic Press, pp. 283–301.
Wang, Y., et al., 2023. PROTAC-mediated selective degradation of cytosolic soluble epoxide hydrolase enhances ER stress reduction. ACS Chem. Biol. 18 (4), 884–896. https://doi.org/10.1021/acschembio.3c00017.
Wilkins, M.R., et al., 1999. Protein identification and analysis tools in the ExPASy server. Methods Mol. Biol. 112, 531–552. https://doi.org/10.1385/1-59259-584-7:531.
Witt, S., Singh, M., Kalisz, H.M., 1998. Structural and kinetic properties of nonglycosylated recombinant Penicillium amagasakiense glucose oxidase expressed in Escherichia coli. Appl. Environ. Microbiol 64 (4), 1405–1411. https://doi.org/10.1128/AEM.64.4.1405-1411.1998.
Yourno, J., Kohno, T., Roth, J.R., 1970. Enzyme evolution: generation of a bifunctional enzyme by fusion of adjacent genes. Nature 228 (5274), 820–824. https://doi.org/10.1038/228820a0.
Zamocky, M., et al., 2008. The peroxidase–cyclooxygenase superfamily: reconstructed evolution of critical enzymes of the innate immune system, 72 (2), 589–605. https://doi.org/10.1002/prot.21950.
Zhang, Y., et al., 2022. Fusion enzyme design based on the "channelization" cascade theory and homogenous dextran product improvement. Int J. Biol. Macromol. 222 (Pt A), 652–660. https://doi.org/10.1016/j.ijbiomac.2022.09.222.
Zhang, Y.H.P., 2011. Substrate channeling and enzyme complexes for biotechnological applications. Biotechnol. Adv. 29 (6), 715–725. https://doi.org/10.1016/j.biotechadv.2011.05.020.